Composites Science and Technology 183 (2019) 107816

Contents lists available at ScienceDirect

Composites Science and Technology

journal homepage: www.elsevier.com/locate/compscitech

Eco-friendly lightweight filament synthesis and mechanical characterization of additively manufactured closed cell foams

Balu Patil[a], B.R. Bharath Kumar[b], Srikanth Bontha[c], Vamsi Krishna Balla[d], Satvasheel Powar[e], V. Hemanth Kumar[f], S.N. Suresha[f], Mrityunjay Doddamani[a,*]

[a] Advanced Manufacturing Laboratory, Department of Mechanical Engineering, National Institute of Technology Karnataka, Surathkal, India
[b] Department of Mechanical Engineering, Jain College of Engineering and Technology, Hubballi, India
[c] Department of Mechanical Engineering, National Institute of Technology Karnataka, Surathkal, 575025, India
[d] Bioceramics and Coating Division, CSIR-Central Glass and Ceramic Research Institute, 196 Raja S.C. Mullick Road, Kolkata, 700 032, West Bengal, India
[e] School of Engineering, Indian Institute of Technology Mandi, Himachal Pradesh, 175005, India
[f] Advanced Asphalt Characterisation and Rheology Laboratory, Department of Civil Engineering, National Institute of Technology Karnataka, India

ARTICLE INFO

Keywords:
Cenospheres
HDPE
Syntactic foam
Filament
3D printing

ABSTRACT

Environmentally pollutant fly ash cenospheres (hollow microballoons) are utilized with most widely consumed, relatively expensive high density polyethylene (HDPE) for developing lightweight eco-friendly filament for 3D printing of closed cell foams. Cenospheres (20, 40 and 60 by volume %) are blended with HDPE and subsequently extruded in filament to be used for 3D printing. Cenosphere/HDPE blends are studied for melt flow index (MFI) and rheological properties. MFI decreases with cenospheres addition. Complex viscosity, storage and loss modulus increase with filler loading. DSC results on the filament and printed samples reveal increasing crystallization temperature and decreasing crystallinity % with no appreciable change in peak melting temperature. Cooling rate variations exhibit crystallinity differences between the filament and the prints. CTE decreases with increasing cenosphere content resulting in lower thermal stresses and under diffusion of raster leading to non-warped prints. Micrography on freeze fractured filament and prints show cenospheres uniform distribution in HDPE. Intact cenospheres lower the foam density making it lightweight. Tensile tests are carried out on filaments and printed samples while flexural properties are investigated for 3D prints. Cenospheres addition resulted in improved tensile modulus and decreased filament strength. Tensile and flexural modulus of printed foams increases with filler content. Results are also compared with injection molded samples. Printed foams registered comparable tensile strength. Specific tensile modulus is noted to be increased with cenospheres loading implying weight saving potential of 3D printed foams. Property map reveals printed foams advantage over other fillers and HDPE composites synthesized through injection and compression molding.

1. Introduction

Fused filament fabrication (FFF) is one of the most widely used additive based manufacturing technique to manufacture prototype and complex functional parts with a very high degree of design freedom compared to traditional manufacturing methods. The choice of the commercially available thermoplastic filaments in FFF is limiting the use of this technology for manufacturig end-use products. Most common thermoplastic polymers like acrylonitrile butadiene styrene [1,2], polyetherimide [3], polylactide [4], polycarbonate [5], polymethylmethacrylate [6] and their blends [7,8] have been used as a feedstock material in commercial FFF printers. Limited studies have been carried out on polymers such as polycaprolactone [9], polybutylene terephthalate [10], polyamide [11], polypropylene [12] and high density polyethylene (HDPE) [13] because of shrinkage/warpage and delamination issues. Recently there is enormous interest seen towards the development, enhancement, and multiplication of feedstock material properties by adding various fillers through different compounding methods. Some of the fillers like carbon and glass fiber [14], iron particles [15], glass [16] and Al_2O_3 powder [17] have been successfully used. Hollow particles such as naturally available fly ash cenospheres and engineered glass microballoon as filler materials in matrix (syntactic foams [18]) are explored well using conventional processing routes wherein tooling cost is higher and have limitations of complex geometrical components [19–21]. These closed cell foams are extensively used in underwater vehicles, thermoforming plugs, aircraft

* Corresponding author.
E-mail address: mrdoddamani@nitk.edu.in (M. Doddamani).

https://doi.org/10.1016/j.compscitech.2019.107816
Received 17 April 2019; Received in revised form 2 July 2019; Accepted 3 September 2019
Available online 04 September 2019
0266-3538/

Nomenclature

ρ	Density	ρ_{th}	Theoretical density
ρ_c	Composite density	$\rho_{\exp}$	Experimental density
ρ_f	Filler density	η'	Complex viscosity
ρ_m	Matrix density	G′	Storage modulus
V_f	Filler volume %	G″	Loss modulus
V_m	Matrix volume %	T_{Melt}	Peak melting temperature
φ_v	Void content	T_{Cryst}	Crystallization temperature
		α_{Cryst}	Degree of crystallinity
		φ_f	Cenospheres volume %

parts and buoys [22] due to their specific properties. The ability to tailor the various properties by selecting different matrix, hollow microballoon configuration and varying volume fraction makes it possible to cater to various applications [23,24]. Particle survival in these foams plays a vital role in determining properties and is dependant on the processing route adopted [25,26]. Such closed cell foam filaments development for weight sensitive structures needs to be addressed and is a worth investigating task. Further, incorporating abundantly available, environmentally pollutant hollow microballoons in relatively expensive widely consumed thermoplastic resin might have an advantage of developing eco-friendly lightweight 3D printed parts.

Producing complex integrated functional parts with fly ash based 3D printed syntactic foams reduce the burden on the environment and can effectively replace relatively expensive HDPE [27–29]. Cenosphere based syntactic foam has superior mechanical properties as compared to neat polymer [30,31]. Alumino-silicate composition in cenospheres compensates property setback caused by surface defects compared to engineered glass microballoon. Despite the defects in fly ash microstructure, the stiffness of their wall material allows their properties within the range of commonly used glass microballoon [32,75,76]. Further, HDPE is the most commonly used semi-crystalline thermoplastic with good flow properties. Owing to its excellent biocompatibility and mechanical response, it is utilized in applications ranging from household utilitarian, milk jugs, packaging industry to structural applications [33,34]. Nonetheless, 3D printing of HDPE and foams therein need shrinkage/warpage, bed adhesion and hollow particle survival issues to be addressed.

Addition of environmentally pollutant hollow fly ash cenospheres makes the feedstock filament to be eco-friendly and can be effectively utilized in smart civil structures [35–37]. Such cenospheres in semi-crystalline HDPE matrix might effectively address warpage issues in realizing utilitarian lightweight 3D printed functional components [13,38]. Retaining the functionality of component with enhanced load-bearing capabilities depend on infill % in 3D prints [39,40]. In the present work, cenosphere/HDPE blends are prepared and investigated for MFI and rheological properties. Developed blends are extruded once to realize eco-friendly lightweight filament and tested for crystallinity and tensile loading condition. Cenospheres/HDPE syntactic foam feedstock filament is subsequently fed to 3D printer and prints are subjected to crystallinity measurement, CTE, tensile and flexural tests. Influence of cenospheres content on the envisaged mechanical properties is presented. Finally, property map is presented and the results of 3D printed samples are compared with the extracted data from the literature. Such property maps help in guiding industrial practitioners to select an appropriate material system based on the applicability in the end-use products.

2. Experimental

2.1. Materials

HDPE (HD50MA180) having an average granular size of 3 mm is procured from Reliance Polymers, Mumbai (Table 1). Fly ash cenospheres (CIL-150) obtained from Cenospheres India Pvt. Ltd., Kolkata are used as fillers without any surface treatment. Sieve and physical analysis details of filler chosen are available in Ref. [41]. As received fly ash cenospheres are sieved to 75 μm to make them pass without any breakage through 0.5 mm nozzle of the 3D printer.

2.2. Blend preparation, MFI, and rheological properties

Blending of HDPE with cenosphere (20, 40 and 60 vol %) is carried out using Brabender (16CME SPL) at 210 °C [22] to get the pellets (Fig. 1a). Blend compositions of 20, 40 and 60 vol% cenospheres in HDPE (H) are represented as H20, H40, and H60 respectively. MFI of as received HDPE and developed cenosphere/HDPE blends are computed using Dynisco LMI5000 laboratory melt flow indexer as per ASTM D1238. Neat HDPE granules and foam pellets obtained from brabender are used for testing. MFI values help in setting appropriate multiplier in the 3D printer for printing foam samples. Rheological properties are important to understand the filler influence on processing conditions. Relative interaction between constituents and rheological behavior of HDPE and foams is carried out using rotational rheometer (Anton Paar rheometer, MCR 502). Frequency sweep test is carried out on a specimen having a dimension of φ 25 × 1 mm at a constant strain rate of 5%. The frequency sweep is conducted at 150 °C in the range of 0.1–10 Hz. Change in complex viscosity (η'), storage (G′) and loss modulus (G″) against frequency and cenospheres content is investigated. For all the tests average of five replicates is presented.

2.3. Filament development and 3D printing

Cenosphere/HDPE pellets (Fig. 1a) are fed into the extruder for fabricating syntactic foam filament. Single screw extruder (25SS/MF/26, L/D ratio of 25:1) from Aasabi Machinery Pvt. Ltd., Mumbai is used to obtain neat HDPE and foam filaments. The temperature profile of 155–160-165-150 °C from the feed to die section is set in the extruder with a constant screw speed of 25 rpm, take-up unit speed of 12.5 rpm to obtain the filaments of diameter 2.85 ± 0.05 mm (Fig. 1b) and is used to feed the 3D printer for printing neat HDPE and foam samples. Neat HDPE and syntactic foam specimens are 3D printed using industrial-scale FFF printer (Star, AHA 3D Innovations, Jaipur) equipped with dual brass nozzles of φ 0.5 mm. Table 2 lists the optimized printing parameters based on cenosphere particle survival, viscosity changes due to filler loading and warpage related issues.

Table 1
Typical Characteristics of HDPE granules*.

Property	Typical Value
MFI (190 °C/2.16 kg)	20.0 g m/10 min.
Density (23 °C)	0.950 g m/cm^3
Tensile Strength at Yield	22 MPa
Elongation at Yield	12%
Flexural Modulus	750 MPa
Notched Izod Impact Strength	30 J/m
Vicat Softening Point	124 °C

*As specified by the supplier.

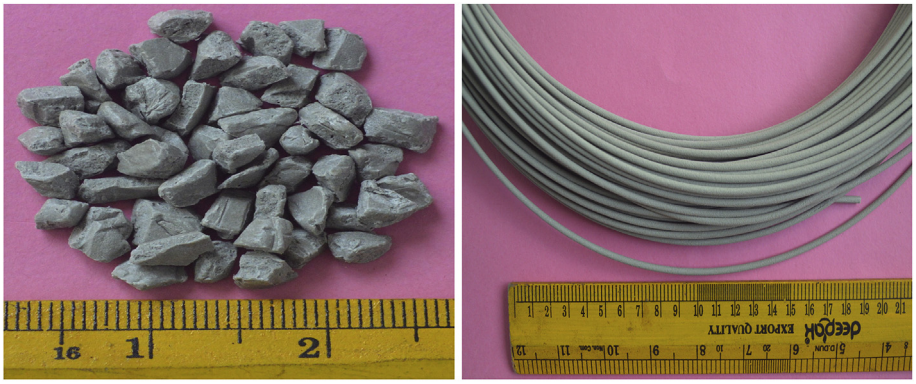

(a) (b)

Fig. 1. (a) Cenospheres/HDPE blend obtained from brabender and (b) representative H60 filament.

Table 2
Printing parameters used in the present work.

Printing parameters	Typical Value
Nozzle temperature (°C)	250
Printing bed temperature (°C)	70
Layer thickness (mm)	0.35
Multiplier	1for H, H20, H40 and 1.2 for H60
Printing speed (mm/sec)	27
Printing pattern	Rectilinear
Part orientation	Y-axis
Infill (%)	100

2.4. Differential scanning calorimeter (DSC) of filament and 3D prints

Melting and the crystallization behavior of the filaments, 3D printed HDPE and foam are analyzed using DSC (PerkinElmer DSC-6000, USA). Sample weighing about 10 mg in 30 µl Al standard crucible is heated from 0 to 200 °C with isothermal curing for 3 min at 200 °C and subsequent cooling to 0 °C at a rate of 10 °C/min. Second heating is performed from 0 to 200 °C after cooling the sample at 0 °C for 3 min. First heating is carried out to nullify the thermal history creeped in because of earlier processing steps. DSC curve typically represents endothermic and exothermic peaks (T_g) and cold crystallization melting enthalpy peak. Crystallinity % (α_{Cryst}) is estimated as,

$$\alpha_{Cryst} = \frac{\Delta H_m}{\Delta H_m^*} \times 100 \tag{1}$$

where, ΔH_m is fusion heat J/g and ΔH_m^* is fusion heat per gram for crystalline HDPE, 293 J/g [42].

2.5. Coefficient of thermal expansion of 3D prints

CTE is the most crucial parameter as far as dimensional stability and part warpage in the FFF process is concerned [43]. CTE of 3D printed specimens is estimated as per ASTM D696-13 using Dilatometer (CIPET, Chennai) and are utilized to correlate the filler loading effect on dimensional stability and microstructure analysis. HDPE and foams are 3D printed to 75 × 12.7 × 3 mm dimension and CTE is performed in 20–90 °C temperature range. Average of five samples are reported for analysis.

2.6. Density and void content

Experimental densities of filaments and printed specimens are measured as per ASTM D792-13. Theoretical density (ρ_{th}) of foams (rule of mixture) is given by,

$$\rho_c = \rho_f V_f + \rho_m V_m \tag{2}$$

where, ρ, *V*, *c*, *f* and *m* represents density, volume fraction, composite, filler and matrix respectively. Voids fraction is given by Ref. [44],

$$\text{Void content}(\varphi_V) = \frac{\rho_{th} - \rho_{exp}}{\rho_{th}} \tag{3}$$

These voids, if present in 3D printed samples indicate air gaps between rasters though infill is 100%. Such air gaps make these prints three-phase foam structure which might be potentially exploited in submarine buoyancy modules.

2.7. Tensile and flexural testing

Tensile tests are performed on filament and 3D prints using Z020 Zwick Roell (USA) UTM (20 kN load cell). Zwick Roell gauge length extensometer (2 inch) is used to record the elongation with 0.1 MPa initial load. The tests are carried out at 5 mm/min as outlined in ASTM D638-14. Flexural testing (pre-load of 0.1 MPa, 1.54 mm/min displacement rate) is carried out on 3D printed samples in three-point bend configuration (ASTM D790-17). Flexural modulus (E_f) is estimated by,

$$E_f = \frac{L^3 m}{4bd^3} \tag{4}$$

where *L*, *m*, *b* and *d* are the span length, slope, sample width and thickness respectively.

Flexural stress (σ_{fm}) is computed using,

$$\sigma_{fm} = \frac{3PL}{2bd^3}(p - load) \tag{5}$$

Micrography on freeze fractured filaments, 3D printed and tested specimens is performed using JSM 6380LA JEOL, Japan by gold sputter coating (JFC-1600) before imaging.

3. Results and discussion

3.1. Melt flow index and rheological behavior of cenosphere/HDPE blends

Flowability of polymer in the molten state is measured using MFI and is inversely proportional to the viscosity. MFI decreases with increasing filler content because of the particles resistance to the polymer flow [45]. Neat HDPE has registered highest MFI (23.06 g m/10 min) as compared to H20 (14), H40 (9.1) and H60 (6.80). MFI decreases by 39.29, 60.54 and 70.51% with increasing cenospheres content of 20, 40 and 60 vol% respectively. A similar trend is reported in Refs. [45,46]. For 3D printing of cenosphere/HDPE foams, reduction in MFI values needs to be compensated either by increasing printing temperature or setting appropriate multiplier factor. The later option is viable to isolate temperature effects and hence printing temperature is kept constant

and the multiplier factor is changed. Fig. 2a present complex viscosity (η') versus frequency for all the samples. Polymer melt viscosity increases with filler infusion [47] and is observed in the complete frequency range. HDPE shows Newtonian-Plateau at a lower angular frequency and the shear thinning region at a higher frequency. H20 exhibit similar behavior with a moderate increase in η'. Whereas for H40 and H60, Newtonian-plateau region is disappeared and only shear thinning is seen for the entire frequency range and is due to more number of polymeric chain entanglements are divided than getting reformed [47]. H60 composition has registered highest η' implying increased viscosity. Cenospheres hinders polymer chain segments mobility making the flow more viscous. Compared to neat HDPE (1080.52 Pa s), viscosity at 0.1 rad/s for H20, H40 and H60 is 1412.42, 2082.10 and 3739.50 Pa s respectively. However, the decrease in η' with frequency is observed for all the coupons. At 50 rad/s the η' of HDPE is about 636.75 Pa s while it's 794.92, 1029.31 and 1558.81 Pa s respectively for H20, H40 and H60. Foams exhibit shear thinning (pseudo plasticity) behavior and are similar to polypropylene-fly ash blend as reported in Ref. [48]. G′ of foams is higher compared to HDPE (Fig. 2b) indicating cenospheres constrain matrix deformation. Storage modulus increases with increasing filler loading leading to foam stiffness enhancement. At lower frequency, neat HDPE and H20 show typical homopolymer-like terminal behavior as HDPE chains are fully relaxed [49]. H20 shows slightly higher modulus compared to neat HDPE. In the case of H40 and H60 composition, a plateau at lower frequency is observed indicating viscoelastic behavior (liquid to solid-like). Also, as frequency increases, the G'the difference between the foams reduces. Loss modulus (G″) is noted to increases with frequency for all samples (Fig. 2c). Also, the addition of cenospheres increased G″. The G″ at 0.1 rad/s is 107.56, 140.37, 205.66 and 370.02 Pa for neat HDPE, H20, H40 and H60 composition respectively. This behavior is due to deformation restrictions caused by the addition of cenospheres.

MFI and rheological behavior results indicate differential parameter choices to be made pertaining to processing conditions and fabrication routes. In this work, the blend is processed through extrusion to get filament (3 mm diameter) and subsequently extruded again to get printed through a nozzle of 0.5 mm diameter. Hence, processing parameters need to be looked into carefully based on MFI and rheological investigations.

3.2. Filament density and microstructure

Quality and behavior of eco-friendly foam feedstock filament are governed by filler-matrix interaction, intact filler and void formations. Sufficient stiffness for spooling and strength (avoid buckling and shearing between the feeding wheels and printer nozzle) are required for the filament to be useable on a 3D printer. Thereby, before using these filaments for 3D printing, their density, morphology and tensile tests are carried out. Table 3 presents densities, void % and weight saving potential data of filament and 3D printed specimens. Voids formed during blending and extrusion (0.34–4.90%) results in three-phase foam structure making them better energy absorbing materials. There is a negligible difference in theoretical and experimental density of HDPE filament indicating the absence of voids. Presence of voids in filament can affect the mechanical properties as they act as a stress concentrator. Void content increases with cenospheres content as seen in Table 3. Due to hydrophobic nature, HDPE did not show any voids post extrusion. Nonetheless, porosity is only observed in foam filament as cenospheres are hydrophilic in nature. Cenospheres primarily comprise of oxides (Al_2O_3 and SiO_2) which links with hydroxyl group resulting in void formation during processing though blends are pre-heated (90 °C) for 24 h. Fig. 3a shows a circular cross-section of freeze-

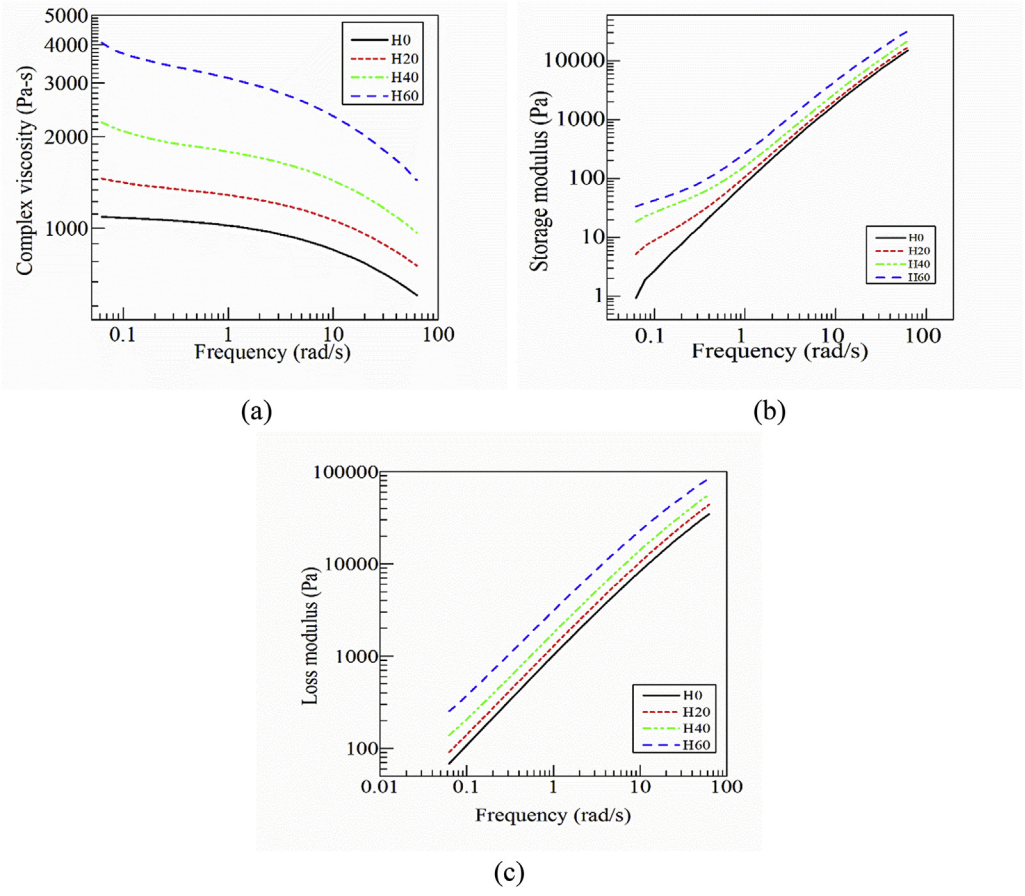

Fig. 2. (a) Complex viscosity (b) storage modulus and (c) loss modulus as a function of frequency for HDPE and their blends.

Table 3
Density, void content and weight saving potential of filament and 3D printed samples.

Material	ϕ_f (vol. %)	ρ_{th} (kg/m^3)	ρ_{exp} (kg/m^3)		ϕ_v (%)		Weight saving potential (%)	
			Filament	3DP	Filament	3DP	Filament	3DP
H	–	950	949.32 ± 15	948.93 ± 23	0.07	0.11	–	–
H20	20	944	940.73 ± 21	938.32 ± 30	0.34	0.60	0.90	1.12
H40	40	938	897.41 ± 29	892.14 ± 37	4.32	4.89	5.47	5.98
H60	60	932	886.28 ± 38	872.11 ± 42	4.90	6.43	6.64	8.10

fractured H20 filament. Fig. 3b shows higher magnification H20 wherein circular pores are formed in the matrix whereas in H40 (Fig. 3c) and H60 (Fig. 3d) larger sized irregular shaped pores are observed. These pores might enhance the damping capabilities of the prints if gets transferred during 3D printing.

3.3. DSC of filament and prints

Degree of crystallinity, melting peak temperature (T_{Melt}) and crystallization temperature (T_{Cryst}) are investigated for both filament and prints for warpage (Table 4). Fig. 4 presents the DSC thermograms of the samples. Compared to HDPE (108 °C) all the foam filaments exhibited gradual increment in T_{Cryst}. Amid HDPE matrix cooling, at comparatively higher temperature melt nucleates on the cenosphere surface forming crystal lamellas of larger thickness resulting in higher T_{Cryst} [50]. 3D prints follow a similar trend. It signifies that additional processing has no significant effect on the crystallization temperature. There is no appreciable change observed in T_{Melt} of the filament and prints indicating the addition of filler and processing step do not influence T_{Melt} (Table 4). Degree of crystallinity (α_{Cryst}) in foam filaments decreases as cenosphere content increases as compared to H (33.15%). Printed specimen follows a similar trend. α_{Cryst} dropped from 57.1 (H) to 39.9% (H60) in prints. Degree of crystallinity is higher in prints compared to their respective filaments which is a welcome sign as far as warpage and dimensional stability of the printed foams. Printed samples are allowed to cool through natural convection mode in the build chamber of the 3D printer while filaments are rapidly cooled in the water bath post extrusion leading to such an observation [51]. Further, as filament gets quenched in a water bath there is not enough time and energy for the melt to crystallize [52]. Drop in α_{Cryst} of foams is due to the hindrance caused by filler particles to the polymer chain movement in addition to the reduction of crystal domain in HDPE [19,53,54] resulting in dimensionally stable foam prints with no warpage. Further, HDPE filament and prints have high crystallinity % and rate due to its linear chain conformation exhibiting prominent warpage while printing. Results presented in Table 4 clearly indicate printing feasibility of cenosphere based lightweight eco-friendly foams for weight sensitive structures.

3.4. Tensile test of filaments

Filament needs to meet a certain requirement to be utilized as feedstock material in the 3D printer without changing functional hardware and software. It must retain its shape without buckling while

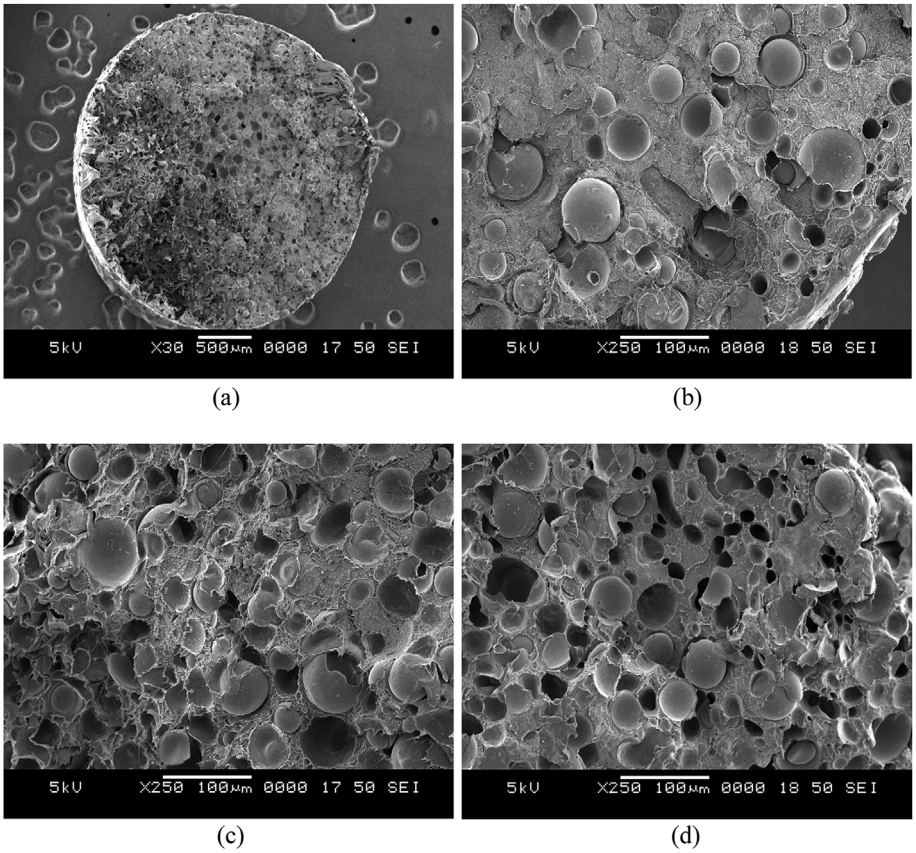

Fig. 3. Freeze fractured micrographs of (a) filament cross section for H20 at lower magnification [74] (b) H20 (c) H40 and (d) H60.

Table 4
T_{Cryst}, α_{Cryst}, T_{Melt} and CTE of samples.

Material	T_{Cryst} (°C)		α_{Cryst} (%)		T_{Melt} (°C)		CTE × 10^{-6} (/°C)	% reduction of CTE w.r.t 'H'
	Filament	3DP	Filament	3DP	Filament	3DP		
H	108.2	109.5	55.5	57.1	131.7	131.2	127 ± 4.29	–
H20	111.4	110.5	43.4	45.6	131.5	130.9	93.2 ± 3.91	26.61
H40	112.5	110.6	41.5	44.8	130.6	129.5	82.4 ± 2.78	35.11
H60	112.6	111.3	37.1	39.9	130.2	129.8	20.3 ± 1.08	84.01

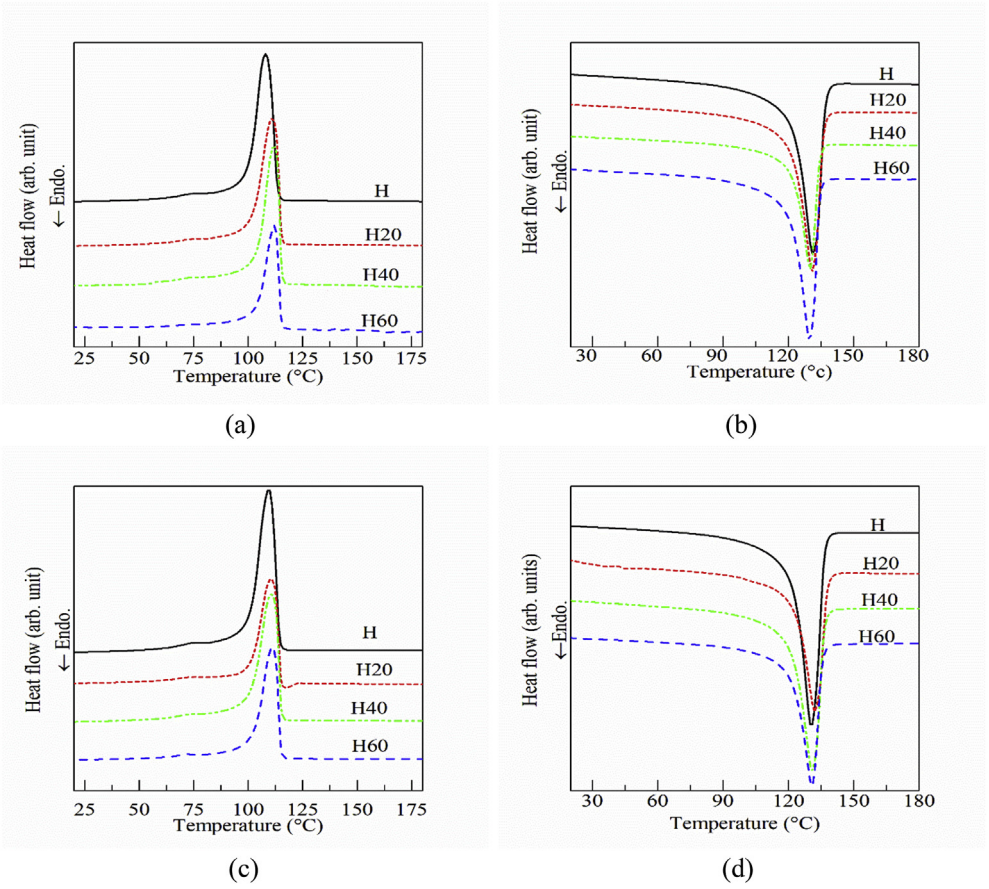

Fig. 4. DSC thermograms for crystallization peak from cooling cycle in (a) filament (c) 3D prints and melting peak from second heating cycle in (b) filament (d) 3D prints.

passing through drive rollers to absorb frictional forces [55]. Buckling can be prevented making the filament stiff enough to resist drive roller push without getting deformed and fractured in the printer head. Higher filler loading increases filament modulus by 7.72–12.79% as compared to HDPE (Table 5). Filament stiffness increases due to stiffer intact cenospheres (Fig. 3) presence in compliant HDPE matrix. Fig. 5 presents representative stress-strain plots (for clarity only up to 30% strain is included) of HDPE and their foam filaments. It is observed that pure HDPE filament undergoes elongation more than 200% strain and the test is discontinued due to time and machine span length constraint. Such higher elongation values without filament failure are due to the ductile nature of HDPE. On the contrary, foam filaments failed within 30% stain. Among the foam filaments, H20 composition registered the highest ultimate strength (10.30 MPa) and strain at break (26.20%). Filament micrography (Fig. 3a) reveal voids across the cross-section of the filament which gets elongated leading to coalesce when pulled under tensile load to get fractured finally. The decreasing trend in strength and break strain is likely due to the incorporation of stiffer

Table 5
Tensile properties of filament and 3D printed material.

Material	Modulus (MPa)		UTS (MPa)		Elongation at UTS (%)		Fracture strength (MPa)		Fracture strain (%)	
	Filament	3DP	Filament	3DP	Filament	3DP	Filament	3DP	Filament	3DP
H	813.26 ± 22	946.20 ± 35	14.90 ± 0.22	18.84 ± 0.28	13.9 ± 0.23	12.99 ± 0.26	–	6.78 ± 0.29	–	142.9 ± 5.89
H20	876.05 ± 31	1125.10 ± 39	10.30 ± 0.34	12.31 ± 0.39	6.70 ± 0.29	5.99 ± 0.33	7.73 ± 0.29	11.45 ± 0.33	26.20 ± 0.15	8.23 ± 0.33
H40	895.19 ± 34	1351.60 ± 44	7.56 ± 0.32	11.25 ± 0.41	3.90 ± 0.31	1.46 ± 0.35	5.34 ± 0.19	10.89 ± 0.25	15.00 ± 0.22	1.51 ± 0.06
H60	971.25 ± 38	1622.37 ± 57	5.62 ± 0.23	12.50 ± 0.53	2.30 ± 0.11	1.44 ± 0.21	4.33 ± 0.14	12.09 ± 0.19	3.30 ± 0.31	1.51 ± 0.07

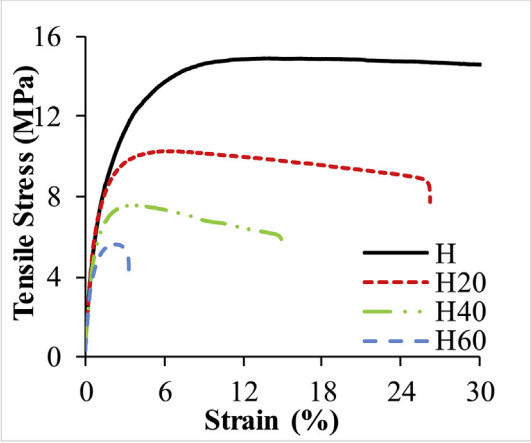

Fig. 5. Representative stress-strain plot of neat HDPE and syntactic foam feedstock filament.

cenospheres and the subsequent reduction in the ductile phase (HDPE).

3.5. Investigations on 3D printed samples

Parameters chosen for 3D printing (Table 2) exhibited seamless interface bonding between the layers (Fig. 6a) and minimum warpage. Post printing, samples are allowed to cool within the enclosed chamber of the 3D printer until the room temperature is reached. Micrographs of freeze-fractured as 3D printed samples for neat HDPE and H60 is presented in Fig. 6b–d. Voids are not seen in neat HDPE (Fig. 6b) while H60 micrograph depicts the uniform distribution of intact cenospheres post printing and elongated voids (Fig. 6c) as mentioned earlier. Density drop in prints compared to HDPE signifies the void content and particle survival post 3D printing process. Void content (Table 3) in printed samples are higher as against the filament owing to the air gaps between bonded adjacent raster (Fig. 6d). These gaps are more prominent at higher filler loadings owing to higher melt viscosity and lower matrix phase. Such additional air gaps in these 3D printed closed cell foams as compared to their filament counterparts results in better weight saving potential (Table 3).

3.6. Coefficient of thermal expansion

Filler addition reduces CTE (Table 4) [56,57]. Incorporation of cenospheres into neat HDPE provides dimensional stability at higher printing temperatures [58]. CTE reduction signifies dimensional stability and lowers thermal stresses resulting in minimized warpage [56]. CTE of cenospheres (3.3×10^{-6}/°C) [56] and HDPE (127×10^{-6}/°C) are quite apart and hence cenospheres loading decreases CTE substantially. CTE values give an insight into raster diffusion mechanism while printing. Part lifting and warpage are observed while printing pure HDPE due to higher CTE. Warpage issues are not encountered while printing foam. It resembles that, the gas of lower thermal conductivity inside hollow cenospheres is restricting the heat flow [58,59]. H60 composition registered lowest CTE indicating minimum molten raster expansion in prints leading to under diffusion of adjacent rasters. As a consequence, the air gap in prints is seen (Fig. 6d). CTE reduction leads to rise in air gaps making 3D printed components to be three-phase foam structures making them lighter than the closed cell foams.

3.7. Tensile behavior

Tensile tested printed samples response is plotted in Fig. 7 and the results are summarized in Table 5. HDPE filament exhibits different response (Fig. 5) as compared to a printed counterpart (Fig. 7a). HDPE filament did not break even after 1000% strain while printed sample failed below 150% strain (Fig. 7a) indicating brittle behavior post printing. A similar observation is noted in foams as well. Neat HDPE shows failure strain over 130% whereas syntactic foam specimens exhibited failure at ~1.5–8%. Neat HDPE underwent plastic deformation

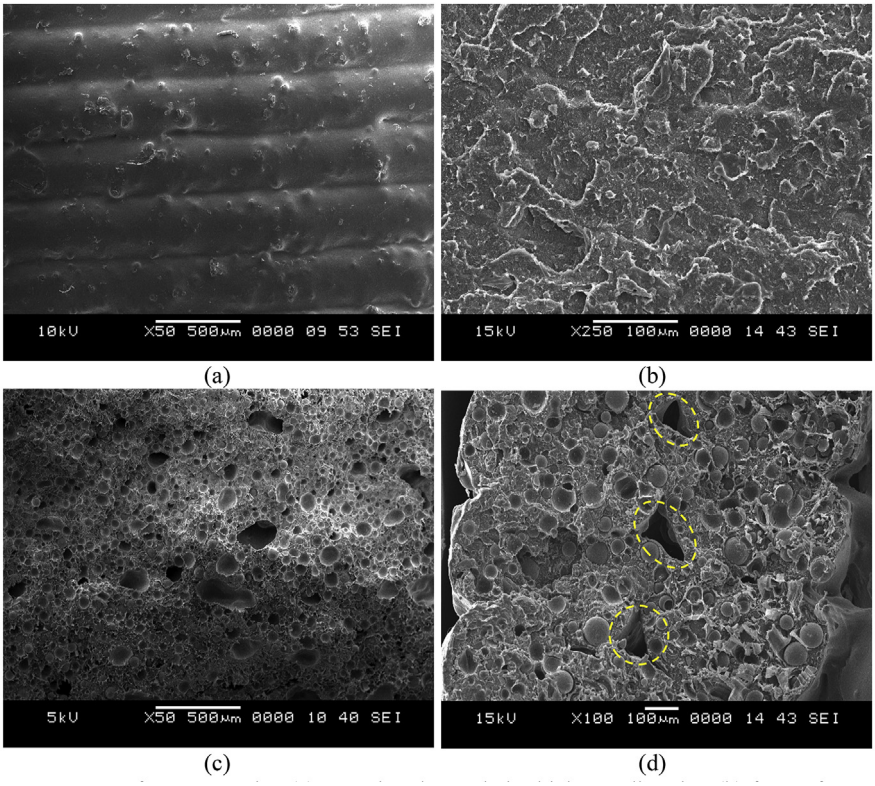

Fig. 6. SEM of representative (a) 3D printed sample in thickness direction (b) freeze fractured HDPE (c) H60 and (d) air gap (marked area) between raster.

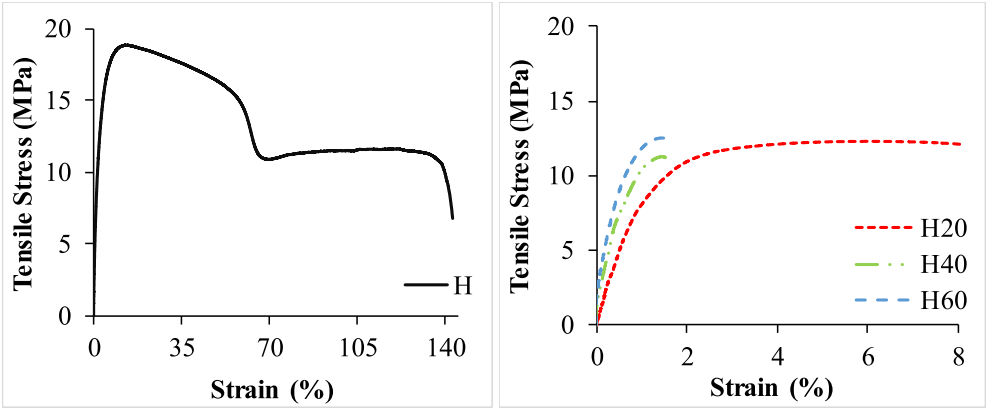

Fig. 7. Representative stress-strain plot for 3D printed (a) HDPE and (b) their foams.

from ~60 to 130% strain. Long necking region is clearly evident in HDPE (Fig. 8a) due to fibrillation of individual raster resulting in broom-like fibrous ends. Printed foam exhibit brittle failure without remarkable plastic deformation (Fig. 8b). Failure of syntactic foam specimens is initiated with plastic deformation of matrix phase at raster planes in the presence of stiff intact cenospheres (Fig. 8c). Infusion of stiffer cenospheres into matrix leads to such behavior. Compared to injection molded HDPE, printed HDPE registered higher elastic modulus (78.86%) with comparable UTS, elongation at ultimate strength and fracture strain while fracture strength gets doubled [60]. Foam modulus increases as filler percentage increases (Table 5). H60 registered the highest modulus among other foam compositions and is 71.46% higher compared to its HDPE counterpart. 3D printed HDPE and foams modulus is 1.16, 1.28, 1.51 and 1.67 times better than the respective feedstock due to the realignment of the polymer chain and additional crosslinking during 3D printing. Modulus of printed cenosphere/HDPE foams is higher in the range of 96.01–144.45% as compared to injection molded ones [60] indicating 3D printing potential in replacing injection molded components with zero lead time and tooling cost. UTS of foams is lower as compared to printed HDPE as constituents are blended without any surface treatment and thereby does not promote interfacial adhesion. UTS and fracture strength of printed material is almost equal to injection molded material [60]. Printed foam registered lower elongation at UTS as compared to injection molded foams. Presence of stiffer cenospheres results in absence of necking and plastic deformation in printed foams (Fig. 8b) and is also reflected in the stress-strain plot (Fig. 7b). Fracture strength of printed foam is 1.78 times higher as compared to neat HDPE. Specific properties of the foams are vital in weight sensitive structures as printing renders the flexibility of integrated components with complex geometry. The specific strength of neat HDPE (0.01985 MPa/(kg/m^3)) is higher as compared to foams (Table 6). H60 registered the highest specific strength among foams. Printed foams have the potential to be used in weight saving the application as depicted by E/ρ, E/ρ^2 and E/ρ^3 values in Table 6.

3.8. Flexural response

Neat HDPE specimen did not show any failure sign up to 10% strain (Fig. 9a) while foams fractured in a brittle manner. Flexural modulus increases with cenosphere content (Table 7) due to intact filler in the HDPE matrix (Fig. 9b). Highest modulus is exhibited by H60 and is 1.56 times better than neat HDPE sample. Strength drop might be due to poor interfacial bonding between constituents and air gaps between the raster. Specific flexural modulus follows the increasing trend with cenospheres percentage. Specific flexural modulus is 1.71 times higher as compared to neat HDPE. 3D printed HDPE showed around 3% higher modulus compared to injection molded foams. H20, H40 and H60 foam registered 25.37, 13.67 and 9.08% lower modulus compared to respective injection molded foams while printed H, H20, H40, and H60 registered 1.62, 1.0, 11.78 and 14.38% lower strength as compared to injection molded ones [22] due to air gaps between adjacent raster in 3D printing as compared to fully dense molded sample.

Tensile and flexural strength decreases with filler loading as surface modification routes are not utilized. Further, amorphous fraction in foams increases as crystallinity decreases with increasing cenosphere content. In turn, cenospheres pose molecular chain mobility and matrix deformation constraints resulting in a weaker interface. Strength might increase in the presence of the coupling agent, despite crystallinity drop (better phase interaction). However, coupling agents might substantially decrease the ductility making filament extrusion and 3D printing quite a challenging task.

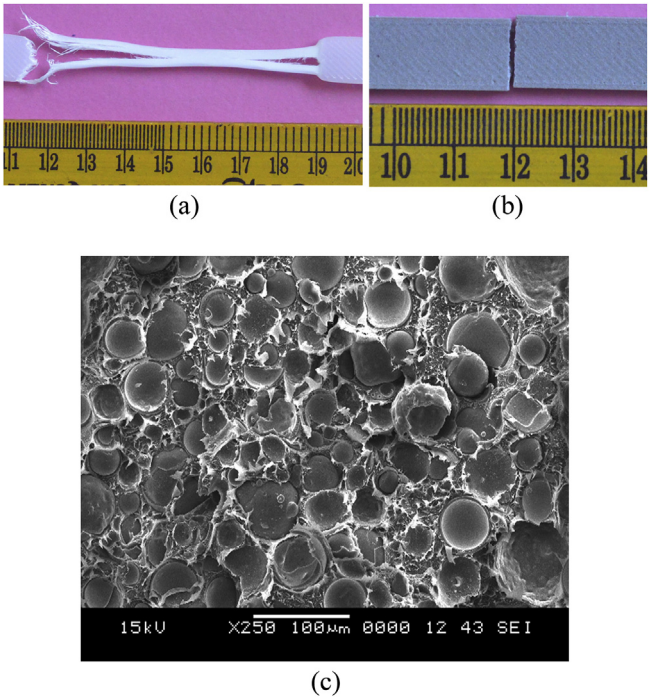

Fig. 8. Representative failed 3D printed sample of (a) HDPE (b) H60 and (c) SEM of H60 post tensile test.

Table 6
Specific properties of syntactic foams fabricated using a 3D printer.

Materials	Specific UTS (MPa/kg/m^3) $\times 10^{-3}$	E/ρ (MPa/kg/m^3)	E/ρ^2 (MPa/(kg/m^3)^2) $\times 10^{-3}$	E/ρ^3 (MPa/(kg/m^3)^3) $\times 10^{-6}$
H	19.85	1.00	1.05	1.11
H20	13.12	1.20	1.28	1.36
H40	12.61	1.52	1.70	1.90
H60	14.33	1.86	2.13	2.45

3.9. Property plots

Tensile and flexural properties data (extracted from literature) are graphed against the HDPE composites density in Fig. 10 [60–68] and Fig. 11 [22,61,62,66,69–73] respectively. It is clear that composites with solid particle reinforcement have higher modulus with a higher density as a common trend. However, hollow particle filled composite provide lower density advantage over solid particles. Present study results show that the density of printed foam falls between compression molded engineered glass microballoon and injection molded cenosphere based closed cell foams. Modulus of printed syntactic foam is higher compared to carbon black, lignocellulose, calcium carbonate, wood, cenospheres, and glass microballoon based systems. Whereas strength is almost comparable with injection and compression molded composites. Flexural modulus of printed foam is lower as compared to injection molded and comparable with compression molded foams. Flexural strength of printed foam is higher as compared to natural fiber and wood powder filled composite, lower compared to injection molded samples and is comparable with compression molded composites. Choice of appropriate extrusion and printing parameters with minimum filler breakage leads to density reduction. By controlling, filler percentage and printing parameters tensile and flexural properties can be exploited well over a wider range.

4. Conclusions

Eco-friendly lightweight cenosphere/HDPE closed cell foam filament is successfully used in FFF based 3D printer. Developed foam filament and prints are analyzed using mechanical tests to address their suitability and feasibility to be utilized for 3D printing applications. Results are summarized as below:

- Cenosphere/HDPE three-phase foam prints without warpage having weight saving potential can be used in marine applications.
- MFI of neat HDPE has decreased with increase in cenospheres content. Rheological results indicate a considerable increase in complex viscosity, loss and storage modulus with increasing cenospheres content.
- Complex viscosities values are maximum at a lower frequency but decrease with an increasing frequency indicating cenospheres/HDPE foams shear thinning behavior. Both storage and loss modulus showed an increasing trend with filler loading and frequency.
- Neat HDPE and foam filaments exhibit lower crystallinity as compared to respective printed material. Filler addition in HDPE matrix reduces CTE remarkably.
- Compared to injection molded HDPE, printed HDPE registered 78.86% higher tensile modulus and two-fold fracture strength. 3D printed HDPE and foams modulus is 1.16, 1.28, 1.51 and 1.67 times better than respective feedstock material. Tensile modulus of prints is higher in the range of 96.01–144.45% as compared to the same composition injection molded ones.
- Flexural modulus increases with cenosphere content. Highest modulus is exhibited by H60 which is 1.56 times better than neat HDPE sample. Air gaps presence lowers flexural modulus and strength as compared to fully dense injection molded samples.
- Property map reveals 3D printing potential over other composites synthesized through different processing routes.

The focus of the present work is to develop eco-friendly lightweight filament for 3D printing of closed cell foams and thereby cater to wide material choices to be offered for the 3D printing industry.

Acknowledgment

Mrityunjay Doddamani acknowledges the Department of Science and Technology, Government of India, Grant DST/TSG/AMT/2015/394/G. S N Suresha would like to acknowledge the financial support extended by the Department of Science and Technology, Government of India under the scheme 'Fund for Improvement of Science & Technology infrastructure' (No.SR/FST/ETI-356/2013) for the creation of required research facilities at the Advanced Asphalt Characterization and Rheology Laboratory, Department of Civil Engineering, NITK, Surathkal.

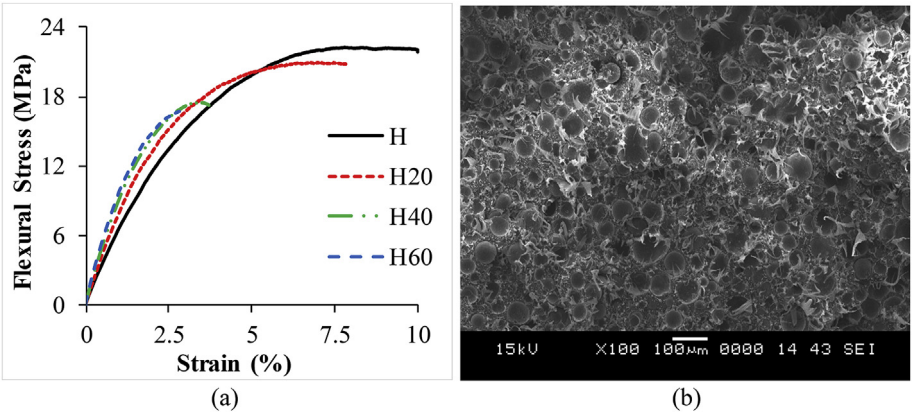

Fig. 9. Representative (a) stress-strain curve for 3D printed samples and (b) micrograph of H60 post flexural test.

Table 7
Flexural properties of printed HDPE and their syntactic foams.

Material	Modulus (MPa)	Strength (MPa)	Fracture strength (MPa)	Fracture strain (%)	Specific modulus (MPa/kg/m^3)	Specific strength (MPa/kg/m^3) × 10^{-3}
H	734.76 ± 31.28	22.24 ± 1.12	–	–	0.77	23.44
H20	883.86 ± 39.56	20.92 ± 1.58	20.80 ± 1.48	7.83 ± 0.19	0.94	22.30
H40	1049.17 ± 41.87	17.48 ± 0.47	17.25 ± 0.41	3.71 ± 0.11	1.18	19.59
H60	1149.28 ± 51.23	16.76 ± 0.72	16.74 ± 0.79	2.97 ± 0.07	1.32	19.22

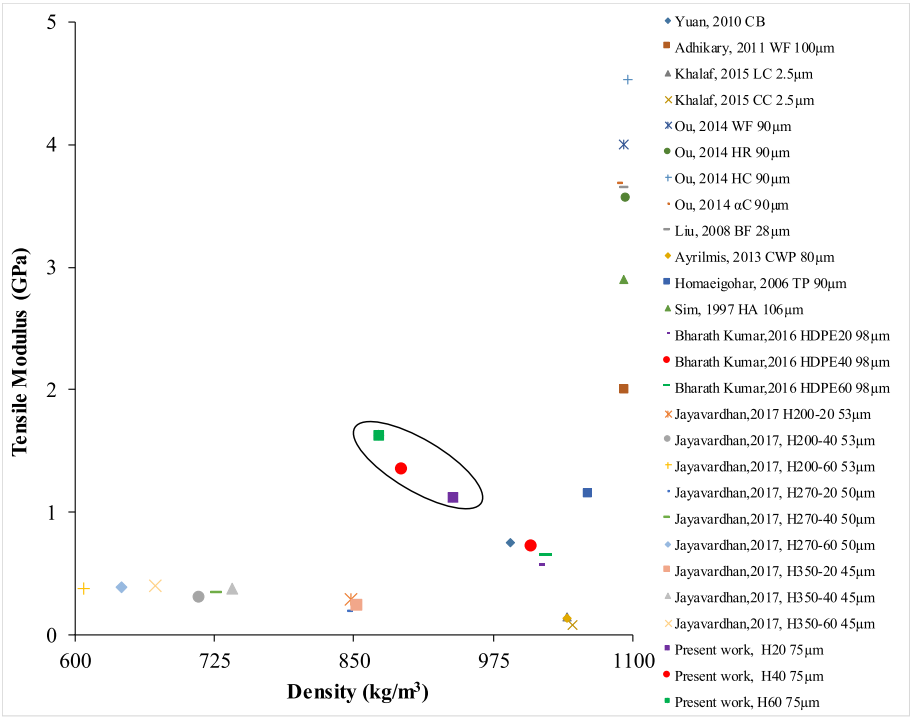

(a)

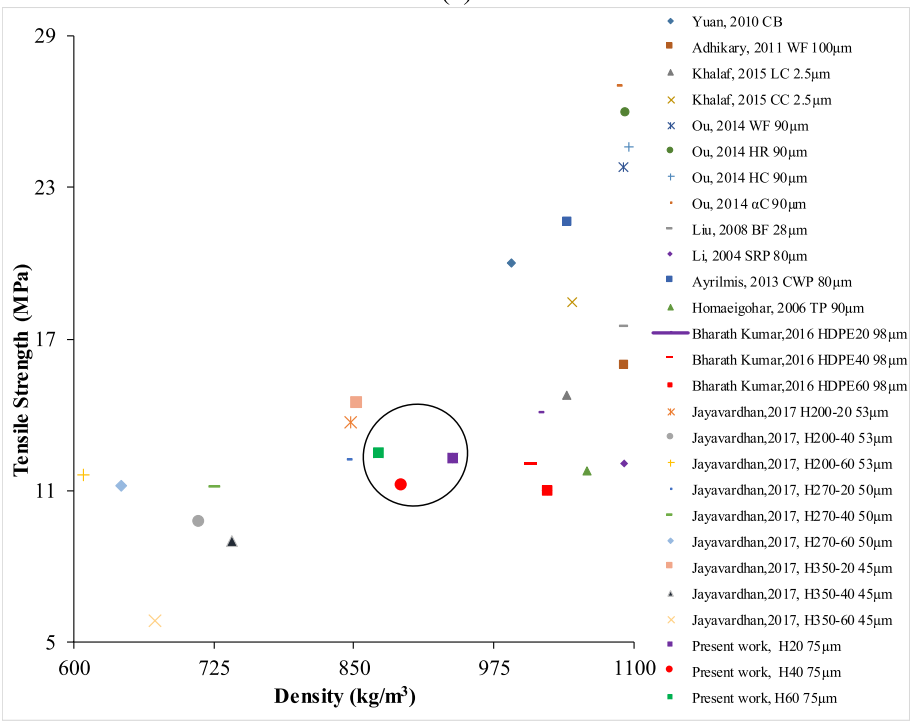

(b)

Fig. 10. (a) Tensile modulus and (b) strength of HDPE composites plotted against density [60–68].

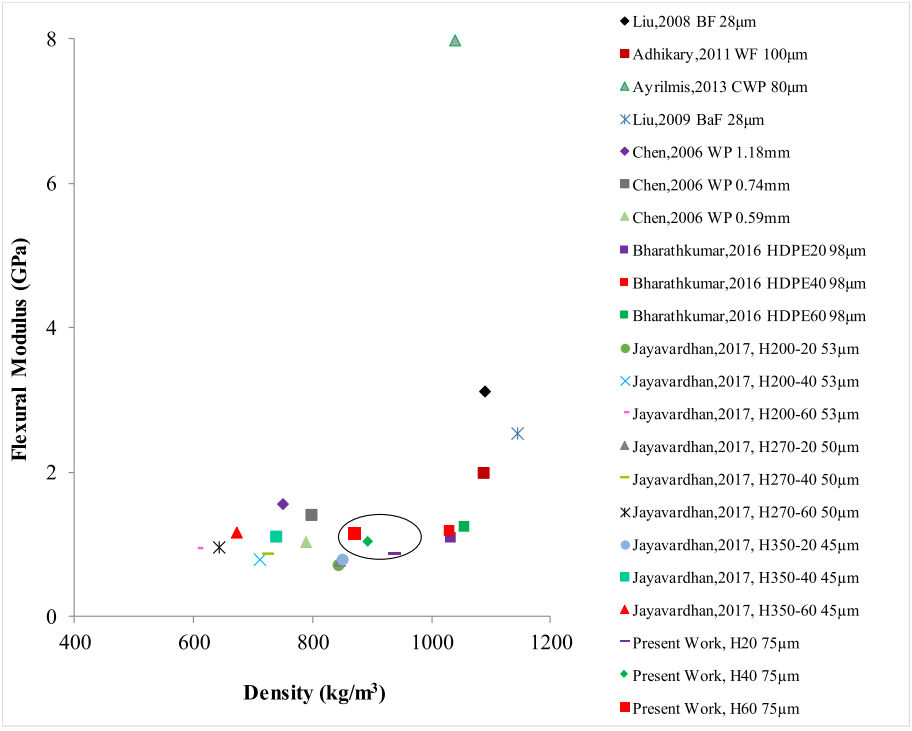

(a)

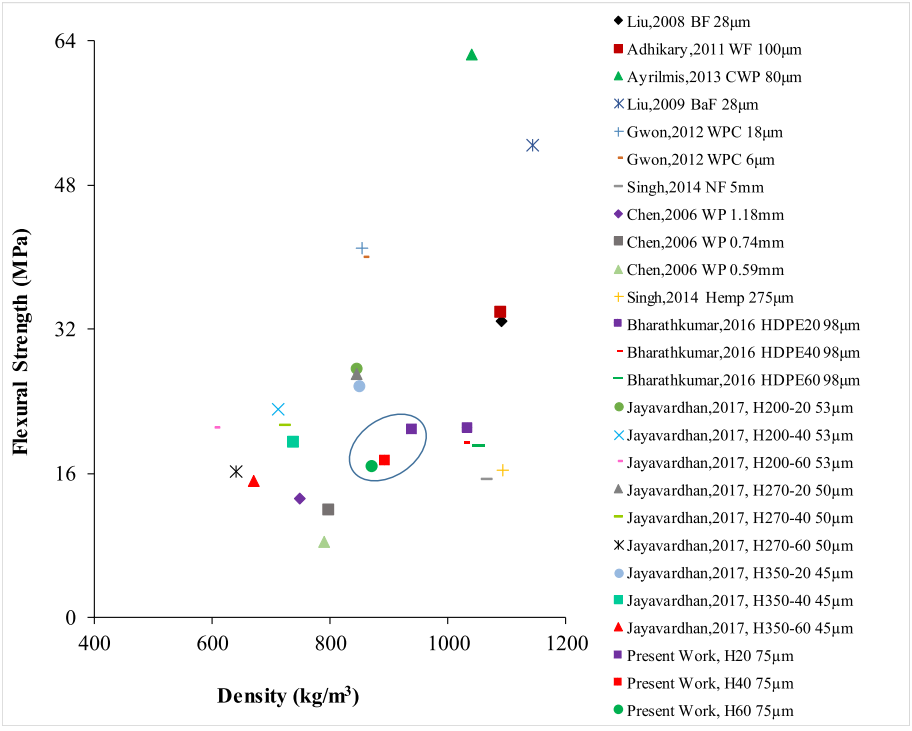

(b)

Fig. 11. (a) Flexural modulus and (b) strength of HDPE composite plotted against density [17,22,61,62,66,69–72].

Appendix A. Supplementary data

Supplementary data to this article can be found online at https://doi.org/10.1016/j.compscitech.2019.107816.

References

[1] B.M. Tymrak, M. Kreiger, J. Pearce, Mechanical properties of components fabricated with open-source 3-D printers under realistic environmental conditions, Mater. Des. 58 (2014) 242–246.
[2] S. Dul, L. Fambri, A. Pegoretti, Fused deposition modelling with ABS–graphene nanocomposites, Compos. Appl. Sci. Manuf. 85 (2016) 181–191.
[3] A. Arivazhagan, A. Saleem, S. Masood, M. Nikzad, K.A. Jagadeesh, Study of dynamic mechanical properties of fused deposition modelling processed ultem material, Am. J. Eng. Appl. Sci. 7 (3) (2014) 307–315.
[4] M. Spoerk, F. Arbeiter, H. Cajner, J. Sapkota, C. Holzer, Parametric optimization of intra- and inter-layer strengths in parts produced by extrusion-based additive manufacturing of poly(lactic acid), J. Appl. Polym. Sci. 134 (41) (2017) 45401.
[5] M. Domingo-Espin, J.M. Puigoriol-Forcada, A.-A. Garcia-Granada, J. Llumà,

S. Borros, G. Reyes, Mechanical property characterization and simulation of fused deposition modeling Polycarbonate parts, Mater. Des. 83 (2015) 670–677.
[6] D. Espalin, K. Arcaute, D. Rodriguez, F. Medina, M. Posner, R. Wicker, Fused deposition modeling of patient-specific polymethylmethacrylate implants, Rapid Prototyp. J. 16 (3) (2010) 164–173.
[7] X. Wang, M. Jiang, Z. Zhou, J. Gou, D. Hui, 3D printing of polymer matrix composites: a review and prospective, Compos. B Eng. 110 (2017) 442–458.
[8] J.W. Stansbury, M.J. Idacavage, 3D printing with polymers: challenges among expanding options and opportunities, Dent. Mater. 32 (1) (2016) 54–64.
[9] Y. Xuan, H. Tang, B. Wu, X. Ding, Z. Lu, W. Li, Z. Xu, A specific groove design for individualized healing in a canine partial sternal defect model by a polycaprolactone/hydroxyapatite scaffold coated with bone marrow stromal cells, J. Biomed. Mater. Res. A 102 (10) (2014) 3401–3408.
[10] B.C. Tellis, J.A. Szivek, C.L. Bliss, D.S. Margolis, R.K. Vaidyanathan, P. Calvert, Trabecular scaffolds created using micro CT guided fused deposition modeling, Mater. Sci. Eng. C 28 (1) (2008) 171–178.
[11] M. Silva, A.M. Pereira, N. Alves, A. Mateus, C. Malça, A hybrid processing approach to the manufacturing of polyamide reinforced parts with carbon fibers, Procedia Manuf. 12 (2017) 195–202.
[12] O. Carneiro, A.F. Silva, R. Gomes, Fused deposition modeling with polypropylene, Mater. Des. 83 (2015) 768–776.
[13] P. Chatkunakasem, P. Luangjuntawong, A. Pongwisuthiruchte, C. Aumnate, P. Potiyaraj, Tuning of HDPE properties for 3D printing, Key Eng. Mater. 773 (2018) 67–71.
[14] B. Brenken, E. Barocio, A. Favaloro, V. Kunc, R.B. Pipes, Fused filament fabrication of fiber-reinforced polymers: a review, Addit. Manuf. 21 (2018) 1–16.
[15] S.H. Masood, W.Q. Song, Development of new metal/polymer materials for rapid tooling using Fused deposition modelling, Mater. Des. 25 (7) (2004) 587–594.
[16] M. Spoerk, F. Arbeiter, I. Raguž, G. Weingrill, T. Fischinger, G. Traxler, S. Schuschnigg, L. Cardon, C. Holzer, Polypropylene filled with glass spheres in extrusion-based additive manufacturing: effect of filler size and printing chamber temperature, Macromol. Mater. Eng. 303 (7) (2018) 1800179.
[17] R. Singh, S. Singh, F. Fraternali, Development of in-house composite wire based feed stock filaments of fused deposition modelling for wear-resistant materials and structures, Compos. B Eng. 98 (2016) 244–249.
[18] F.A. Shutov, Syntactic Polymer Foams, Springer Berlin Heidelberg, Berlin, Heidelberg, 1986.
[19] M.V. D, M. Sharma, S. Rrn, A. P, P. Sampathkumaran, S. Seetharamu, Mechanical and thermal characteristics of high density polyethylene–fly ash Cenospheres composites, Mater. Des. 31 (2010) 2051–2060.
[20] S.N. Patankar, Y.A. Kranov, Hollow glass microsphere HDPE composites for low energy sustainability, Mater. Sci. Eng. A 527 (6) (2010) 1361–1366.
[21] S.N. Patankar, A. Das, Y.A. Kranov, Interface engineering via compatibilization in HDPE composite reinforced with sodium borosilicate hollow glass microspheres, Compos. Appl. Sci. Manuf. 40 (6) (2009) 897–903.
[22] Bharath Kumar, B. R, M. Doddamani, S. Zeltmann, N. Gupta, Uzma, S. Gurupadu, S. RRN, Effect of particle surface treatment and blending method on flexural properties of injection-molded cenosphere/HDPE syntactic foams, J. Mater. Sci. 51 (8) (2016) 3793–3805.
[23] M.L. Jayavardhan, M. Doddamani, Quasi-static compressive response of compression molded glass microballoon/HDPE syntactic foam, Compos. B Eng. 149 (2018) 165–177.
[24] N. Gupta, W. Ricci, Comparison of compressive properties of layered syntactic foams having gradient in microballoon volume fraction and wall thickness, Mater. Sci. Eng. A 427 (1) (2006) 331–342.
[25] Bharath Kumar, B. R, M. Doddamani, S.E. Zeltmann, N. Gupta, M.R. Ramesh, S. Ramakrishna, Processing of cenosphere/HDPE syntactic foams using an industrial scale polymer injection molding machine, Mater. Des. 92 (2016) 414–423.
[26] M.L. Jayavardhan, B.R. Bharath Kumar, M. Doddamani, A.K. Singh, S.E. Zeltmann, N. Gupta, Development of glass microballoon/HDPE syntactic foams by compression molding, Compos. B Eng. 130 (2017) 119–131.
[27] N. Gupta, B. Singh Brar, E. Woldesenbet, Effect of filler addition on the compressive and impact properties of glass fibre reinforced epoxy, Bull. Mater. Sci. 24 (2) (2001) 219–223.
[28] B.K. Satapathy, A. Das, A. Patnaik, Ductile-to-brittle transition in cenosphere-filled polypropylene composites, J. Mater. Sci. 46 (6) (2011) 1963–1974.
[29] J. Qiao, G. Wu, Tensile properties of fly ash/polyurea composites, J. Mater. Sci. 46 (11) (2011) 3935–3941.
[30] B. Bharath Kumar, S.E. Zeltmann, M. Doddamani, N. Gupta, S. Gurupadu, R. Sailaja, Effect of cenosphere surface treatment and blending method on the tensile properties of thermoplastic matrix syntactic foams, J. Appl. Polym. Sci. 133 (35) (2016).
[31] B.R.B. Kumar, M. Doddamani, S.E. Zeltmann, N. Gupta, S. Ramakrishna, Data characterizing tensile behavior of cenosphere/HDPE syntactic foam, Data in Brief 6 (2016) 933–941.
[32] C.D. Garcia, K. Shahapurkar, M. Doddamani, G.C.M. Kumar, P. Prabhakar, Effect of arctic environment on flexural behavior of fly ash cenosphere reinforced epoxy syntactic foams, Compos. B Eng. 151 (2018) 265–273.
[33] K. Chrissafis, K.M. Paraskevopoulos, I. Tsiaoussis, D. Bikiaris, Comparative study of the effect of different nanoparticles on the mechanical properties, permeability, and thermal degradation mechanism of HDPE, J. Appl. Polym. Sci. 114 (3) (2009) 1606–1618.
[34] O.Y. Alothman, Processing and characterization of high density polyethylene/ethylene vinyl acetate blends with different VA contents, Adv. Mater. Sci. Eng. 2012 (2012) 10.
[35] F. Fabbrocino, I. Farina, A. Amendola, L. Feo, F. Fraternali, Optimal design and additive manufacturing of novel reinforcing elements for composite materials, VII European Congress on Computational Methods in Applied Sciences and Engineering, Crete Island, Greece, 2016.
[36] F. Fraternali, G. Carpentieri, R. Montuori, A. Amendola, G. Benzoni, On the use of mechanical metamaterials for innovative seismic isolation systems, COMPDYN 2015 - 5th ECCOMAS Thematic Conference on Computational Methods in Structural Dynamics and Earthquake Engineering, Crete Island, Greece, 2015.
[37] A. Amendola, F. Fabbrocino, L. Feo, F. Auricchio, F. Fraternali, Dependence of the mechanical properties of pentamode materials on the lattice microstructure, VII European Congress on Computational Methods in Applied Sciences and Engineering, Crete Island, Greece, 2016.
[38] S. Chong, G.-T. Pan, M. Khalid, T.C.-K. Yang, S.-T. Hung, C.-M. Huang, Physical characterization and pre-assessment of recycled high-density polyethylene as 3D printing material, J. Polym. Environ. 25 (2) (2017) 136–145.
[39] A.K. Singh, B. Patil, N. Hoffmann, B. Saltonstall, M. Doddamani, N. Gupta, Additive manufacturing of syntactic foams: Part 1: development, properties, and recycling potential of filaments, JOM 70 (3) (2018) 303–309 https://doi.org/10.1007/s11837-017-2734-7.
[40] A.K. Singh, B. Saltonstall, B. Patil, N. Hoffmann, M. Doddamani, N. Gupta, Additive manufacturing of syntactic foams: Part 2: specimen printing and mechanical property characterization, JOM 70 (3) (2018) 310–314 https://doi.org/10.1007/s11837-017-2731-x.
[41] S. Waddar, J. Pitchaimani, M. Doddamani, N. Gupta, Buckling and free vibration behavior of cenosphere/epoxy syntactic foams under axial compressive loading, Mater. Perform. Char. 7 (1) (2018) 532–546.
[42] V.C. Divya, V.V. Pattanshetti, R. Suresh, R.R.N. Sailaja, Development and characterisation of HDPE/EPDM-g-TMEVS blends for mechanical and morphological properties for engineering applications, J. Polym. Res. 20 (2) (2013) 51.
[43] E.R. Fitzharris, N. Watanabe, D.W. Rosen, M.L. Shofner, Effects of material properties on warpage in fused deposition modeling parts, Int. J. Adv. Manuf. Technol. 95 (5) (2018) 2059–2070.
[44] N. Gupta, E. Woldesenbet, P. Mensah, Compression properties of syntactic foams: effect of cenosphere radius ratio and specimen aspect ratio, Compos. Appl. Sci. Manuf. 35 (1) (2003) 103–111.
[45] Viviane Alves Escócio, Elen Beatriz Acordi Vasques Pacheco, Ana Lucia Nazareth da Silva, André de Paula Cavalcante, L.L.Y. Visconte, Rheological behavior of renewable polyethylene (HDPE) composites and sponge gourd (Luffa cylindrica) residue, Int. J. Polym. Sci. 2015 (2015) 7.
[46] S. Mohanty, S.K. Nayak, Short bamboo fiber-reinforced HDPE composites: influence of fiber content and modification on strength of the composite, J. Reinf. Plast. Compos. 29 (14) (2010) 2199–2210.
[47] H. Shaikh, A. Anis, A.M. Poulose, M. Alam, M.N. A-Otaibi, M.A. Alam, S.M. Al-Zahrani, Studies on high density polyethylene reinforced with phosphate ore particles: thermal, rheological, mechanical and morphological properties, Polym. Plast. Technol. Eng. 55 (17) (2016) 1831–1841.
[48] S.G. Pardo, C. Bernal, A. Ares, M.J. Abad, J. Cano, Rheological, thermal, and mechanical characterization of fly ash-thermoplastic composites with different coupling agents, Polym. Compos. 31 (10) (2010) 1722–1730.
[49] M. El Achaby, H. Ennajih, F.Z. Arrakhiz, A. El Kadib, R. Bouhfid, E. Essassi, A. Qaiss, Modification of montmorillonite by novel geminal benzimidazolium surfactant and its use for the preparation of polymer organoclay nanocomposites, Compos. B Eng. 51 (2013) 310–317.
[50] A. Anis, A.M. Poulose, M. Alam, M.N. A-Otaibi, M.A. Alam, S.M. Al-Zahrani, Studies on high density polyethylene reinforced with phosphate ore particles: thermal, rheological, mechanical and morphological properties AU - shaikh, Polym. Plast. Technol. Eng. 55 (17) (2016) 1831–1841.
[51] A. Wasiak, P. Sajkiewicz, A. Woźniak, Effects of cooling rate on crystallinity of i-polypropylene and polyethylene terephthalate crystallized in nonisothermal conditions, J. Polym. Sci. B Polym. Phys. 37 (20) (1999) 2821–2827.
[52] C. Yang, X. Tian, D. Li, Y. Cao, F. Zhao, C. Shi, Influence of thermal processing conditions in 3D printing on the crystallinity and mechanical properties of PEEK material, J. Mater. Process. Technol. 248 (2017) 1–7.
[53] P. Panupakorn, E. Chaichana, P. Praserthdam, B. Jongsomjit, Polyethylene/clay nanocomposites produced by in situ polymerization with zirconocene/MAO catalyst, J. Nanomater. 2013 (2013) 9.
[54] K. Sewda, S.N. Maiti, Crystallization and melting behavior of HDPE in HDPE/teak wood flour composites and their correlation with mechanical properties, J. Appl. Polym. Sci. 118 (4) (2010) 2264–2275.
[55] J.L. Lombardi, R.A. Hoffinan, J.A. Waters, D. Popovich, Issues associated with EFF & FDM ceramic filled feedstock formulation, 1997 International Solid Freeform Fabrication Symposium, 1997.
[56] S. Baglari, M. Kole, T.K. Dey, Effective thermal conductivity and coefficient of linear thermal expansion of high-density polyethylene — fly ash composites, Indian J. Phys. 85 (4) (2011) 559–573.
[57] V.C. Shunmugasamy, D. Pinisetty, N. Gupta, Thermal expansion behavior of hollow glass particle/vinyl ester composites, J. Mater. Sci. 47 (14) (2012) 5596–5604.
[58] M. Labella, S.E. Zeltmann, V.C. Shunmugasamy, N. Gupta, P.K. Rohatgi, Mechanical and thermal properties of fly ash/vinyl ester syntactic foams, Fuel 121 (2014) 240–249.
[59] M. Atagür, M. Sarikanat, T. Uysalman, O. Polat, İ.Y. Elbeyli, Y. Seki, K. Sever, Mechanical, thermal, and viscoelastic investigations on expanded perlite–filled high-density polyethylene composite, J. Elastomers Plastics 50 (8) (2018) 747–761.
[60] Bharath Kumar, B. R, M. Doddamani, S. Zeltmann, N. Gupta, M.R. Ramesh, S. Ramakrishna, Processing of cenosphere/HDPE syntactic foams using an industrial scale polymer injection molding machine, Mater. Des. 92 (2016) 414–423.
[61] K.B. Adhikary, C.B. Park, M.R. Islam, G.M. Rizvi, Effects of lubricant content on extrusion processing and mechanical properties of wood flour-high-density

polyethylene composites, J. Thermoplast. Compos. Mater. 24 (2) (2011) 155–171.
[62] N. Ayrilmis, Combined effects of boron and compatibilizer on dimensional stability and mechanical properties of wood/HDPE composites, Compos. B Eng. 44 (1) (2013) 745–749.
[63] M.N. Khalaf, Mechanical properties of filled high density polyethylene, J. Saudi Chem. Soc. 19 (1) (2015) 88–91.
[64] S.S. Homaeigohar, A.Y. Sadi, J. Javadpour, A. Khavandi, The effect of reinforcement volume fraction and particle size on the mechanical properties of β-tricalcium phosphate–high density polyethylene composites, J. Eur. Ceram. Soc. 26 (3) (2006) 273–278.
[65] C.P. Sim, P. Cheang, M.H. Liang, K.A. Khor, Injection moulding of hydroxyapatite composites, J. Mater. Process. Technol. 69 (1) (1997) 75–78.
[66] H. Liu, Q. Wu, G. Han, F. Yao, Y. Kojima, S. Suzuki, Compatibilizing and toughening bamboo flour-filled HDPE composites: mechanical properties and morphologies, Compos. Appl. Sci. Manuf. 39 (12) (2008) 1891–1900.
[67] Q. Yuan, S.A. Bateman, D. Wu, Mechanical and conductive properties of carbon black-filled high-density polyethylene, low-density polyethylene, and linear low-density polyethylene, J. Thermoplast. Compos. Mater. 23 (4) (2010) 459–471.
[68] R. Ou, Y. Xie, M.P. Wolcott, S. Sui, Q. Wang, Morphology, mechanical properties, and dimensional stability of wood particle/high density polyethylene composites: effect of removal of wood cell wall composition, Mater. Des. 58 (2014) 339–345.
[69] H. Liu, Q. Wu, Q. Zhang, Preparation and properties of banana fiber-reinforced composites based on high density polyethylene (HDPE)/Nylon-6 blends, Bioresour. Technol. 100 (23) (2009) 6088–6097.
[70] J.G. Gwon, S.Y. Lee, H. Kang, J.H. Kim, Effects of sizes and contents of exothermic foaming agent on physical properties of injection foamed wood fiber/HDPE composites, Int. J. Precis. Eng. Manuf. 13 (6) (2012) 1003–1007.
[71] H.C. Chen, T.Y. Chen, C.H. Hsu, Effects of wood particle size and mixing ratios of HDPE on the properties of the composites, Holz Roh Werkst. 64 (3) (2006) 172–177.
[72] M. Sood, Investigation of Flexural behavior of hybrid natural fiber composite with recycled polymer matrix, Am. Int. J. Res. Sci. Technol. Eng. Math. 6 (3) (2014) 237–240.
[73] S. Singh, D. Deepak, L. Aggarwal, V.K. Gupta, Tensile and flexural behavior of hemp fiber reinforced virgin-recycled HDPE matrix composites, Procedia Mater. Sci. 6 (2014) 1696–1702.
[74] B. Patil, B.K. B. R., M. Doddamani, Compressive behavior of fly ash based 3D printed syntactic foam composite, Materials Letters 254 (2019) 246–249 https://doi.org/10.1016/j.matlet.2019.07.080.
[75] K. Shahapurkar, C.D. Garcia, M. Doddamani, G.C. Mohan Kumar, P. Prabhakar, Compressive behavior of cenosphere/epoxy syntactic foams in arctic conditions, Composites Part B: Engineering 135 (2018) 253–262 https://doi.org/10.1016/j.compositesb.2017.10.006.
[76] V. Manakari, G. Parande, M. Doddamani, M. Gupta, Enhancing the Ignition, Hardness and Compressive Response of Magnesium by Reinforcing with Hollow Glass Microballoons, Materials 10 (9) (2017) 1–15 https://doi.org/10.3390/ma10090997.